

Blood-pressure-induced oscillations of deoxy- and oxyhemoglobin concentrations are in-phase in the healthy breast and out-of-phase in the healthy brain

Kristen T. Tgavalekos
Jana M. Kainerstorfer
Angelo Sassaroli
Sergio Fantini

Blood-pressure-induced oscillations of deoxy- and oxyhemoglobin concentrations are in-phase in the healthy breast and out-of-phase in the healthy brain

Kristen T. Tgavalekos,* Jana M. Kainerstorfer,† Angelo Sassaroli, and Sergio Fantini

Tufts University, Department of Biomedical Engineering, 4 Colby Street, Medford, Massachusetts 02155, United States

Abstract. We present a near-infrared spectroscopy (NIRS) study of local hemodynamics in the breast and the brain (prefrontal cortex) of healthy volunteers in a protocol involving periodic perturbations to the systemic arterial blood pressure. These periodic perturbations were achieved by cyclic inflation (to a pressure of 200 mmHg) and deflation (at frequencies of 0.046, 0.056, 0.063, 0.071, and 0.083 Hz) of two pneumatic cuffs wrapped around the subject's thighs. As a result of these systemic perturbations, the concentrations of deoxy- and oxyhemoglobin in tissue (D and O , respectively) oscillate at the set frequency. We found that the oscillations of D and O in breast tissue are in-phase at all frequencies considered, a result that we attribute to dominant contributions from blood volume oscillations. In contrast, D and O oscillations in brain tissue feature a frequency-dependent phase difference, which we attribute to significant contributions from cerebral blood flow oscillations. Frequency-resolved measurements of D and O oscillations are exploited by the technique of coherent hemodynamics spectroscopy for the assessment of cerebrovascular parameters and cerebral autoregulation. We show the relevant physiological information content of NIRS measurements of oscillatory hemodynamics, which have qualitatively distinct features in the healthy breast and healthy brain. © The Authors. Published by SPIE under a Creative Commons Attribution 3.0 Unported License. Distribution or reproduction of this work in whole or in part requires full attribution of the original publication, including its DOI. [DOI: [10.1117/1.JBO.21.10.101410](https://doi.org/10.1117/1.JBO.21.10.101410)]

Keywords: near-infrared spectroscopy; hemodynamic oscillations; blood volume; blood flow; coherent hemodynamics spectroscopy. Paper 150683SSR received Oct. 13, 2015; accepted for publication Mar. 3, 2016; published online Mar. 28, 2016.

1 Introduction

Near-infrared spectroscopy (NIRS) is a noninvasive optical method for local measurements of deoxyhemoglobin (D) and oxyhemoglobin (O) concentrations in tissue and has been used for a variety of applications such as functional brain imaging¹ and breast cancer imaging.^{2,3} Recently, there has been interest in spontaneous as well as induced oscillations of D and O , because their amplitudes and relative phases can be related to physiological quantities such as blood volume, blood flow, oxygen consumption, and cerebral autoregulation (AR). Oscillations of D and O occur naturally within the human body at the heart rate (~ 1 Hz), the respiratory rate (~ 0.25 Hz), and at the frequency of spontaneous low-frequency oscillations (~ 0.1 Hz). Oscillations can also be induced at specific frequencies with various protocols, including paced breathing,⁴ thigh cuff occlusions,⁵ and squat-stand maneuvers.⁶

The phase difference between D and O oscillations is relevant to the study of both the diseased and healthy human brains. In a brain study of patients with unilateral carotid obstruction, it was found that, in a paced breathing protocol, the phase lag between D and O oscillations was significantly larger on the side with the obstruction than on the contralateral healthy side.⁷ These findings were attributed to impaired versus normal cerebral AR, the mechanism that maintains cerebral

blood flow in response to changes in the mean arterial pressure (MAP). In a sleep study of healthy subjects, NIRS measurements from the brain revealed altered phase differences between D and O low-frequency (~ 0.1 Hz) spontaneous oscillations when comparing non-rapid eye movement (REM) with REM sleep states,⁸ a finding that was interpreted in terms of oscillations in blood flow velocity and blood volume.

Coherent hemodynamics spectroscopy (CHS) is a method for studying hemodynamic physiological processes and tissue oxygen consumption in terms of the phases and amplitudes of deoxyhemoglobin, oxyhemoglobin, and total hemoglobin (T) concentrations at multiple frequencies of oscillations.⁹ The amplitude and phase of D , O , and T oscillations at angular frequency ω can be described with phasor notation: $\mathbf{D}(\omega)$, $\mathbf{O}(\omega)$, and $\mathbf{T}(\omega)$. CHS spectra are given by the frequency dependence of the magnitude and phase of the phasor ratios $\mathbf{D}(\omega)/\mathbf{O}(\omega)$ and $\mathbf{O}(\omega)/\mathbf{T}(\omega)$. In phasor algebra, this corresponds to the following amplitude ratios and phase differences as a function of frequency: $|\mathbf{D}|/|\mathbf{O}|$, $|\mathbf{O}|/|\mathbf{T}|$, $\text{Arg}(\mathbf{D}) - \text{Arg}(\mathbf{O})$, and $\text{Arg}(\mathbf{O}) - \text{Arg}(\mathbf{T})$, where "Arg" is the argument of the phasor, i.e., its phase angle with respect to the x -axis. By means of a hemodynamic model,⁹ the measured CHS spectra can be related to fundamental physiological parameters like the capillary and venous blood transit times and the cutoff frequency of the cerebral AR process.

CHS can be applied to any tissue, not just the brain. In this study, we have also chosen to study the breast tissue, because CHS may yield valuable information for cancer assessment as a result of the hemodynamic and metabolic perturbations associated with breast cancer. The utility of assessing hemodynamic

*Address all correspondence to: Kristen T. Tgavalekos, E-mail: kristen.tgavalekos@tufts.edu

†Present address: Carnegie Mellon University, Department of Biomedical Engineering, 700 Technology Drive, Pittsburgh, Pennsylvania 15219, United States

changes with NIRS in breast tissue has been investigated in the literature. In a study looking at breast hemodynamics, a dual-breast near-infrared tomographic system measured different responses to a Valsalva maneuver in a comparison between the healthy and tumor-bearing breasts on the same subject.¹⁰ The return to baseline of deoxyhemoglobin concentration in the tumor-bearing breast lagged behind the return to baseline in the healthy breast. Carp et al.¹¹ have studied the breast hemodynamic response to compression in order to investigate physiological differences of healthy and diseased tissues. Breast hemodynamics during periodic oscillations have also been studied with a protocol in which subjects used a respiratory device to alternate between breathing oxygen and carbogen.¹² Total hemoglobin concentration response was measured with NIRS, and the reported results support that the total hemoglobin responses of cancerous breasts were less correlated to the changes in inspired oxygen concentrations than the total hemoglobin responses of healthy breasts. Flexman et al.¹³ have studied the response of breast tissue to a breath-holding protocol and found differences between malignant and healthy tissues during breath holding and recovery. The spatial and temporal study of breast hemodynamics may result in a powerful tool for the characterization and detection of abnormalities in the tissue vasculature and metabolism. CHS may therefore be a useful addition to this area of study.

Oscillations in blood volume and blood flow have individual effects on the oscillations of D and O that are measured with NIRS. Blood volume oscillations, by themselves, result in synchronous (or in-phase) oscillations of D and O . Blood flow oscillations, by themselves, result in oscillations of D and O that are in opposition of phase (π -phase difference). Such individual volume and flow effects are, in general, out-of-phase with each other even in the case in which the blood volume and blood flow oscillations are synchronous. This result follows from the delayed D and O responses to blood flow changes (this delay is caused by the finite blood transit time in the microvasculature), which we modeled by treating the microvasculature as a low-pass filter for the driving blood flow dynamics (input) and the resulting D and O dynamics (output).⁹ According to this analysis, the phase difference between the overall, measured D and O oscillations reflects the relative contributions to

them from blood volume and blood flow changes. In-phase D and O oscillations suggest volume-dominated effects, and opposition-of-phase D and O oscillations suggest flow-dominated effects. The relative contributions to D and O oscillations from oscillations in blood volume and blood flow (and, when applicable, oxygen consumption) may depend on the frequency of oscillations, and this fact is exploited by CHS for a quantitative study of tissue hemodynamics and oxidative metabolism.⁹

Even though blood volume and blood flow changes may be interconnected (e.g., a change in blood volume in a compartment may reflect an imbalance between flow in and flow out of that compartment), we note that NIRS is not sensitive to blood flow dynamics occurring outside the capillary compartment. One of the assumptions of our model is that blood volume changes occur synchronously in the three compartments (arterial, capillary, and venous), and for this reason, we use the general term “blood volume change” without any further clarification. On the contrary, blood flow changes in the context of this work refer only to capillary flow changes.

In this study, we have used NIRS to concurrently measure blood-pressure-induced hemoglobin oscillations in the breast and the brain (prefrontal cortex) of healthy volunteers. The measured CHS spectra in the breast and the brain show that D and O oscillations are in-phase (i.e., synchronous) in the healthy breast and out-of-phase (i.e., asynchronous) in the healthy brain. We attribute these results to different relative contributions of blood volume and blood flow to the measured oscillations of D and O in the two tissues examined. While we have focused on breast and brain tissues, a similar hemodynamic study in other tissues can yield similar information about the contribution of blood volume and blood flow to hemoglobin concentration oscillations measured with NIRS.

2 Methods

2.1 Human Subjects and Data Acquisition

Eleven healthy female subjects (age range: 24 to 32 years old) participated in the study. All subjects were premenopausal, had no history of vascular disorders, and had no known risks for breast cancer. The Tufts University Institutional Review Board approved the experimental protocol, and the subjects provided

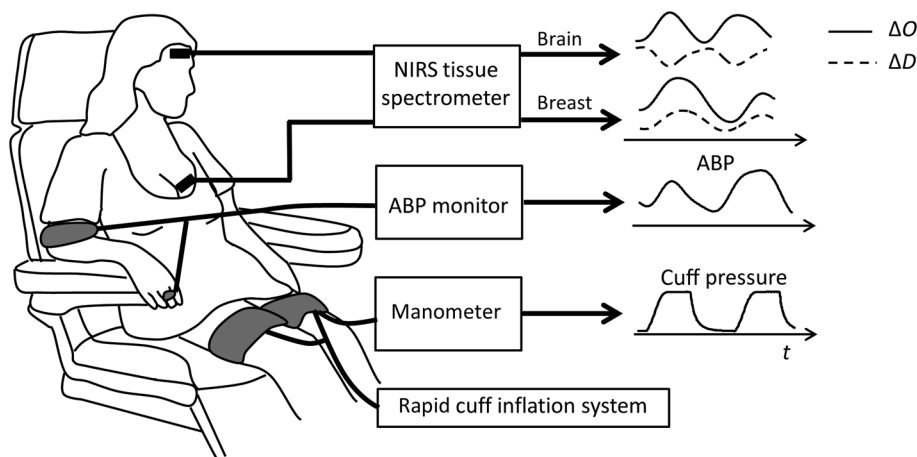


Fig. 1 Experimental setup. Signals from the NIRS instrument, ABP monitor, and thigh cuff manometer were recorded synchronously. Optical data from the spectrometer were used to compute the changes in O and D (ΔO and ΔD) over time (t).

written informed consent prior to the experiment. Figure 1 shows the experimental setup. The NIRS measurements were performed with a frequency-domain commercial NIRS instrument (OxiplexTS, ISS Inc., Champaign, Illinois). Optical probes connected to the spectrometer delivered light at two wavelengths, 690 and 830 nm, at a source–detector distance of 35 mm. The brain probe was placed against the left side of the subject’s forehead, to access tissue in the prefrontal cortex, and secured with a flexible headband. The breast probe was placed ~20 mm above the areola of the left breast and secured with adhesive medical tape. Continuous arterial blood pressure (ABP) was recorded with a beat-to-beat blood pressure monitoring system (NIBP100D, BIOPAC Systems, Inc., Goleta, California). Pneumatic thigh cuffs were wrapped around both of the subject’s thighs and connected to an automated cuff inflation system (E-20 Rapid Cuff Inflation System, D.E. Hokanson, Inc., Bellevue, Washington). The air pressure in the thigh cuffs was continuously monitored with a digital manometer (Series 626 Pressure Transmitter, Dwyer Instruments, Inc., Michigan City, Indiana). Analog outputs of the ABP monitor and the thigh cuff pressure monitor were fed to auxiliary inputs of the NIRS instrument for concurrent recordings with the NIRS data. All signals were sampled synchronously at an acquisition rate of 12.5 Hz.

Baseline measurements, during which the subjects were resting and the thigh cuffs were deflated, were recorded for 2 min for each participant. Then the thigh cuffs were periodically inflated (to a pressure of ~200 mmHg) and deflated for six periods at five different frequencies, f_i ($f_i = \omega_i/2\pi$): 0.046, 0.056, 0.063, 0.071, and 0.083 Hz. The cyclic inflations of the thigh cuffs induced periodic changes in the ABP.⁵ The associated changes in O and D in the brain and breast were measured with NIRS. Each set of cyclic cuff inflations was followed by 20 s of rest during which the baseline conditions were re-established.

2.2 Data Analysis

Data analysis and processing were performed with MATLAB® (Mathworks Inc., Natick, Massachusetts). Optical intensity changes from the brain and the breast were translated to changes in the concentrations of oxyhemoglobin [$\Delta O(t)$], deoxyhemoglobin [$\Delta D(t)$], and total hemoglobin [$\Delta T(t)$] using the modified Beer–Lambert law. The signals were analyzed with the following process for each of the five frequencies of thigh cuff oscillations, f_i ($i = 1, \dots, 5$). The time traces were filtered with a linear phase, finite impulse response, bandpass filter based on the Parks–McClellan algorithm.¹⁴ The filter had a width of 0.01 Hz that was centered at f_i . The Hilbert transform was applied to the bandpass-filtered signals in order to obtain the instantaneous amplitude and phase at that frequency.¹⁵ Experiments on tissue-like phantoms with static optical properties were used to determine the noise floor of the intensity measurements, which were translated to the detection threshold for oscillations in hemoglobin concentrations in tissue. From these phantom experiments, a threshold of 0.015 μM was considered the noise level for the amplitude of oscillations and applied to the instantaneous amplitudes of deoxy- and oxyhemoglobin to remove data points with lower amplitudes.¹⁶ The thigh cuff manometer signal was then used to determine the time ranges at which the six periods of induced oscillations of frequency f_i occurred. The magnitudes and phases of $\mathbf{D}(\omega_i)/\mathbf{O}(\omega_i)$ and $\mathbf{O}(\omega_i)/\mathbf{T}(\omega_i)$ were computed and averaged within the time ranges of the measurements at each f_i to obtain CHS spectra [namely $|\mathbf{D}|/|\mathbf{O}|$, $|\mathbf{O}|/|\mathbf{T}|$, $\text{Arg}(\mathbf{D}) - \text{Arg}(\mathbf{O})$, and $\text{Arg}(\mathbf{O}) - \text{Arg}(\mathbf{T})$].

In the case of brain measurements, the CHS spectra showed typical features previously reported by our group¹⁷ and allowed for the assessment of six hemodynamic parameters by fitting the CHS spectra with a hemodynamic model.⁹ Briefly, the model describes how \mathbf{O} , \mathbf{D} , and \mathbf{T} are related to microcirculation blood volume, blood flow, and metabolic rate of oxygen. The key equations for the model are

$$\frac{\mathbf{D}(\omega)}{\mathbf{O}(\omega)} = \frac{(1 - S^{(a)}) \frac{\text{CBV}_0^{(a)} \mathbf{cbv}^{(a)}(\omega)}{\text{CBV}_0^{(v)} \mathbf{cbv}^{(v)}(\omega)} + (1 - S^{(v)}) - \left[\frac{\langle S^{(c)} \rangle (\langle S^{(c)} \rangle - S^{(v)})}{S^{(v)}} \frac{\mathcal{F}^{(c)} \text{CBV}_0^{(c)}}{\text{CBV}_0^{(v)}} \mathcal{H}_{\text{RC-LP}}^{(c)}(\omega) + (S^{(a)} - S^{(v)}) \mathcal{H}_{\text{G-LP}}^{(v)}(\omega) \right] k \frac{\text{CBV}_0^{(v)}}{\text{CBV}_0^{(a)}} \mathcal{H}_{\text{RC-HP}}^{(\text{AR})}(\omega) \left[\frac{\text{CBV}_0^{(a)} \mathbf{cbv}^{(a)}(\omega)}{\text{CBV}_0^{(v)} \mathbf{cbv}^{(v)}(\omega)} + 1 \right]}{S^{(a)} \frac{\text{CBV}_0^{(a)} \mathbf{cbv}^{(a)}(\omega)}{\text{CBV}_0^{(v)} \mathbf{cbv}^{(v)}(\omega)} + S^{(v)} + \left[\frac{\langle S^{(c)} \rangle (\langle S^{(c)} \rangle - S^{(v)})}{S^{(v)}} \frac{\mathcal{F}^{(c)} \text{CBV}_0^{(c)}}{\text{CBV}_0^{(v)}} \mathcal{H}_{\text{RC-LP}}^{(c)}(\omega) + (S^{(a)} - S^{(v)}) \mathcal{H}_{\text{G-LP}}^{(v)}(\omega) \right] k \frac{\text{CBV}_0^{(v)}}{\text{CBV}_0^{(a)}} \mathcal{H}_{\text{RC-HP}}^{(\text{AR})}(\omega) \left[\frac{\text{CBV}_0^{(a)} \mathbf{cbv}^{(a)}(\omega)}{\text{CBV}_0^{(v)} \mathbf{cbv}^{(v)}(\omega)} + 1 \right]}, \quad (1)$$

$$\frac{\mathbf{O}(\omega)}{\mathbf{T}(\omega)} = \frac{S^{(a)} \frac{\text{CBV}_0^{(a)} \mathbf{cbv}^{(a)}(\omega)}{\text{CBV}_0^{(v)} \mathbf{cbv}^{(v)}(\omega)} + S^{(v)} + \left[\frac{\langle S^{(c)} \rangle (\langle S^{(c)} \rangle - S^{(v)})}{S^{(v)}} \frac{\mathcal{F}^{(c)} \text{CBV}_0^{(c)}}{\text{CBV}_0^{(v)}} \mathcal{H}_{\text{RC-LP}}^{(c)}(\omega) + (S^{(a)} - S^{(v)}) \mathcal{H}_{\text{G-LP}}^{(v)}(\omega) \right] k \frac{\text{CBV}_0^{(v)}}{\text{CBV}_0^{(a)}} \mathcal{H}_{\text{RC-HP}}^{(\text{AR})}(\omega) \left[\frac{\text{CBV}_0^{(a)} \mathbf{cbv}^{(a)}(\omega)}{\text{CBV}_0^{(v)} \mathbf{cbv}^{(v)}(\omega)} + 1 \right]}{\frac{\text{CBV}_0^{(a)} \mathbf{cbv}^{(a)}(\omega)}{\text{CBV}_0^{(v)} \mathbf{cbv}^{(v)}(\omega)} + 1}, \quad (2)$$

where S and its superscripts describe the oxygen saturation of hemoglobin in the arterial (a), capillary (c), or venous (v) compartment, and $\langle S^{(c)} \rangle$ denotes a spatial average of the capillary saturation. The phasor that describes the oscillations of cerebral blood volume $\mathbf{cbv}(\omega)$ and baseline

cerebral blood volume CBV_0 may also have superscripts to indicate their values for a specific vascular compartment. The Fåhræus factor $\mathcal{F}^{(c)}$ accounts for reduced hematocrit in the capillaries. Three transfer functions are notated as \mathcal{H} with subscript and superscript specifiers of the nature of the

filter and vascular compartment (if applicable): RC low-pass (RC-LP) in the capillary compartment, Gaussian low-pass (G-LP) in the venous compartment, and RC high-pass (RC-HP) for AR.⁹ We used a nonlinear fitting procedure in MATLAB (function “lsqcurvefit”) with a trust region reflective algorithm to fit our measurements with the model. The six hemodynamic parameters fitted for in our analysis are the capillary blood transit time ($t^{(c)}$), the venous blood transit time ($t^{(v)}$), the ratio of capillary-to-venous baseline blood volumes corrected for the small-to-large vessel hematocrit ratio ($\mathcal{F}^{(c)}\text{CBV}_0^{(c)}/\text{CBV}_0^{(v)}$), the ratio of amplitudes of arterial-to-venous blood volume oscillations ($\Delta\text{CBV}^{(a)}/\Delta\text{CBV}^{(v)}$), the AR cutoff frequency (f_c^{AR}), and the product of the inverse of the Grubb’s exponent (k) times the ratio of venous-to-total baseline blood

volumes ($k\text{CBV}_0^{(v)}/\text{CBV}_0$). The search regions for the fitting parameters are defined by ranges found in the literature.¹⁸ The analytical expressions derived from the hemodynamic model and the simplifying assumptions relating these six hemodynamic parameters and the CHS spectra are described in detail in Kainerstorfer et al.¹⁹

In the case of breast measurements, because the phasors $\mathbf{D}(\omega_i)$, $\mathbf{O}(\omega_i)$, and $\mathbf{T}(\omega_i)$ were found to be in-phase with each other at all measured frequencies, the amplitude ratio $|\mathbf{O}(\omega_i)|/|\mathbf{T}(\omega_i)|$ provides a measure of the oxygen saturation of hemoglobin in the volume-oscillating vascular compartments,⁹ which we indicate here with S_V . This measure of hemoglobin saturation is a weighted average of the saturations of the volume-oscillating compartments, where each vascular compartment is weighted according to its relative contributions to the overall blood volume oscillations:

$$S_V = \frac{\text{CBV}_0^{(a)}|\mathbf{cbv}^{(a)}(\omega)|S^{(a)} + \mathcal{F}^{(c)}\text{CBV}_0^{(c)}|\mathbf{cbv}^{(c)}(\omega)|\langle S^{(c)} \rangle + \text{CBV}_0^{(v)}|\mathbf{cbv}^{(v)}(\omega)|S^{(v)}}{\text{CBV}_0|\mathbf{cbv}(\omega)|}. \quad (3)$$

3 Results

Figure 2 shows the bandpass-filtered time traces of changes in ABP, O , and D in the brain and the breast for subject no. 8. By inspection of Fig. 2, one can clearly see the oscillations in systemic ABP and local concentrations of oxy- and deoxyhemoglobin that are elicited by the cyclic thigh cuff occlusions (identified by the vertical gray bars in Fig. 2).

The group averages of CHS spectra were computed for the 11 subjects. A variance threshold was used to select the induced frequencies in each subject that successfully maintained a consistent phase difference: the standard deviation of $\text{Arg}(\mathbf{D}) - \text{Arg}(\mathbf{O})$ and the standard deviation of $\text{Arg}(\mathbf{O}) - \text{Arg}(\mathbf{T})$ both needed to be $<45^\circ$. The number of subjects for whom the measured data passed the threshold was as follows for brain data at each

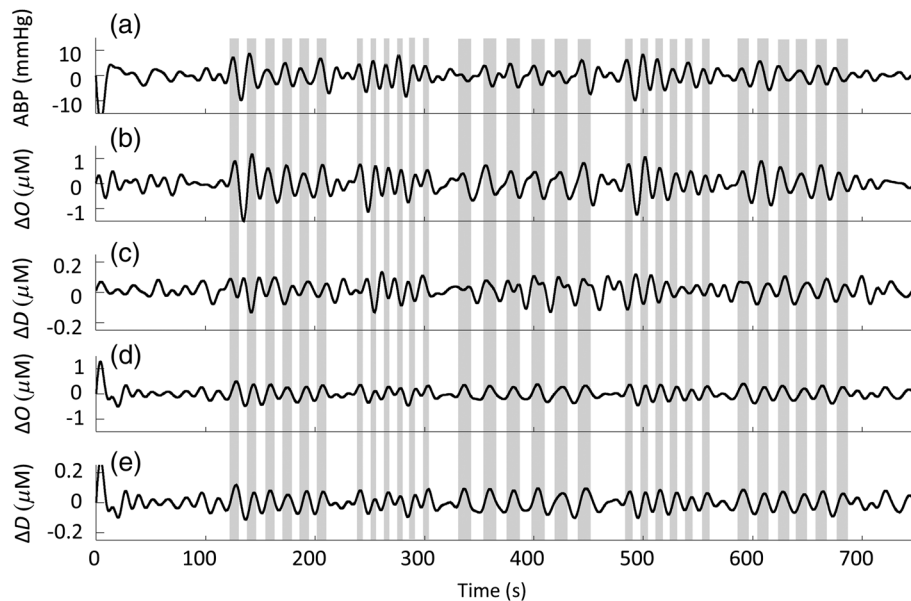


Fig. 2 Time traces for subject no. 8. The shaded regions indicate the times at which the cuffs were inflated to a pressure of 200 mmHg. The cuffs were timed such that each frequency has six periods for analysis. The order of frequencies in this figure is: 0.063, 0.083, 0.046, 0.071, and 0.056 Hz. (a) Changes in mean ABP; (b) changes in oxyhemoglobin concentration measured in brain tissue; (c) changes in deoxyhemoglobin concentration measured in brain tissue; (d) changes in oxyhemoglobin concentration measured in breast tissue; and (e) changes in deoxyhemoglobin concentration measured in breast tissue. All the temporal traces shown in this figure were bandpass filtered (0.01 to 0.11 Hz, width: 0.1 Hz), whereas data analysis at each frequency was performed by applying a narrower bandpass filter (width: 0.01 Hz) centered at the frequency of interest.

frequency: 0.046 Hz, $n = 10$; 0.056 Hz, $n = 11$; 0.063 Hz, $n = 10$; 0.071 Hz, $n = 10$; and 0.083 Hz, $n = 11$. For breast data, the corresponding numbers of subjects were as follows: 0.046 Hz, $n = 11$; 0.056 Hz, $n = 11$; 0.063 Hz, $n = 11$; 0.071 Hz, $n = 11$; and 0.083 Hz, $n = 10$. On almost all the subjects and all the frequencies, we could measure reliable and coherent hemodynamics on both brain and breast tissues. For the cases that passed the threshold requirement, the mean phase differences and amplitude ratios (representing the CHS spectra) were computed and are shown in Fig. 3. To compute the mean values and standard deviations of $\text{Arg}(\mathbf{D}) - \text{Arg}(\mathbf{O})$ and $\text{Arg}(\mathbf{O}) - \text{Arg}(\mathbf{T})$, we used the standard methods in circular statistics.²⁰ For $|\mathbf{D}|/|\mathbf{O}|$ and $|\mathbf{O}|/|\mathbf{T}|$, we computed the group means, and the errors bars in Fig. 3 represent the standard error of the mean.

For the brain spectra, the best fits with the hemodynamic model are also plotted (solid lines in Fig. 3). The brain CHS spectra show quantitative features similar to those found in previous measurements in healthy subjects.¹⁷ Over the frequency range measured here (0.046 to 0.083 Hz), the phase spectrum for $\text{Arg}(\mathbf{D}) - \text{Arg}(\mathbf{O})$ shows a negative slope of ~ 0.8 deg/mHz, whereas the amplitude spectra have values of ~ 0.25 for $|\mathbf{D}|/|\mathbf{O}|$ and ~ 1.2 for $|\mathbf{O}|/|\mathbf{T}|$ (we observe that $|\mathbf{O}|/|\mathbf{T}|$ is a phasor amplitude ratio, so that its value > 1 is not incompatible with the phasor relationship $\mathbf{T} = \mathbf{O} + \mathbf{D}$). The oscillations of D lag behind the oscillations of O by 210 deg to 235 deg, whereas the oscillations of O lag behind the oscillations of T by 5 deg to 10 deg.

The CHS spectra measured in the breast did not show frequency dependence for any of the subjects, and a horizontal straight line at the value of the mean for each spectrum is shown in Fig. 3 (dashed lines). The mean of $\text{Arg}(\mathbf{D}) - \text{Arg}(\mathbf{O})$ is $2 \text{ deg} \pm 14 \text{ deg}$ and the mean of $\text{Arg}(\mathbf{O}) - \text{Arg}(\mathbf{T})$ is $0 \text{ deg} \pm 2 \text{ deg}$, both of which indicate a nonsignificant difference from zero, so that the oscillations of O , D , and T in the breast can be described to be in-phase. The mean value of

$|\mathbf{D}|/|\mathbf{O}|$ is 0.21 ± 0.01 , whereas the mean value of $|\mathbf{O}|/|\mathbf{T}|$ is 0.83 ± 0.01 (in this case of in-phase \mathbf{D} , \mathbf{O} , and \mathbf{T} phasors, the ratio $|\mathbf{O}|/|\mathbf{T}|$ must be ≤ 1).

The phase difference between the oscillations of deoxy- and oxyhemoglobin concentrations [$\text{Arg}(\mathbf{D}) - \text{Arg}(\mathbf{O})$] was the feature of greatest interest for this study, because it provides dynamic information about the relative contributions of volume and flow changes in the probed tissue. As an illustrative example of the phase difference of D and O oscillations, Fig. 4(a) shows the time traces of D and O changes (ΔD and ΔO) and Fig. 4(b) shows the corresponding phasor diagrams of \mathbf{D} and \mathbf{O} . Figure 4 refers to subject no. 1 and a frequency of cyclic cuff inflation of 0.056 Hz [the time periods of cuff inflation are shaded in Fig. 4(a)]. The time traces in Fig. 4(a) show the out-of-phase behavior of deoxy- and oxyhemoglobin oscillations in brain tissue (top panels of Fig. 4) and the in-phase behavior of the oscillations in breast tissue (bottom panels of Fig. 4). In this example, $\text{Arg}(\mathbf{D}) - \text{Arg}(\mathbf{O})$ is $-185 \text{ deg} \pm 2 \text{ deg}$ in the brain and $4 \text{ deg} \pm 1 \text{ deg}$ in the breast. In Fig. 4(b), \mathbf{O} is the phase reference (set at 0 deg), and the phasor amplitudes are drawn to scale with respect to each other.

The fits to the brain CHS spectra with the hemodynamic model (solid lines in Fig. 3) yielded the set of six hemodynamic parameters defined in Sec. 2.2. The mean values of these parameters (\pm the standard error of the mean) over the 11 subjects were as follows: $t^{(c)} = 0.9 \pm 0.2 \text{ s}$, $t^{(v)} = 5.4 \pm 1.1 \text{ s}$, $(\mathcal{F}^{(c)}\text{CBV}_0^{(c)}/\text{CBV}_0^{(v)}) = 1.3 \pm 0.3$, $(\Delta\text{CBV}^{(a)}/\Delta\text{CBV}^{(v)}) = 5.2 \pm 1.7$, $f_c^{(\text{AR})} = 0.03 \pm 0.02 \text{ Hz}$, $(k\text{CBV}_0^{(v)}/\text{CBV}_0) = 0.8 \pm 0.2$. Most parameters are in good agreement with values previously reported for the prefrontal cortex of 11 healthy human subjects during a paced breathing protocol.¹⁹ Specifically, the previously reported values of the six parameters were $0.9 \pm 0.2 \text{ s}$, $1.3 \pm 0.3 \text{ s}$, 1.1 ± 0.3 , 2.9 ± 0.9 , $0.035 \pm 0.002 \text{ Hz}$, and 0.6 ± 0.1 , respectively.¹⁹ While some of the parameters deviate from our previous results, the

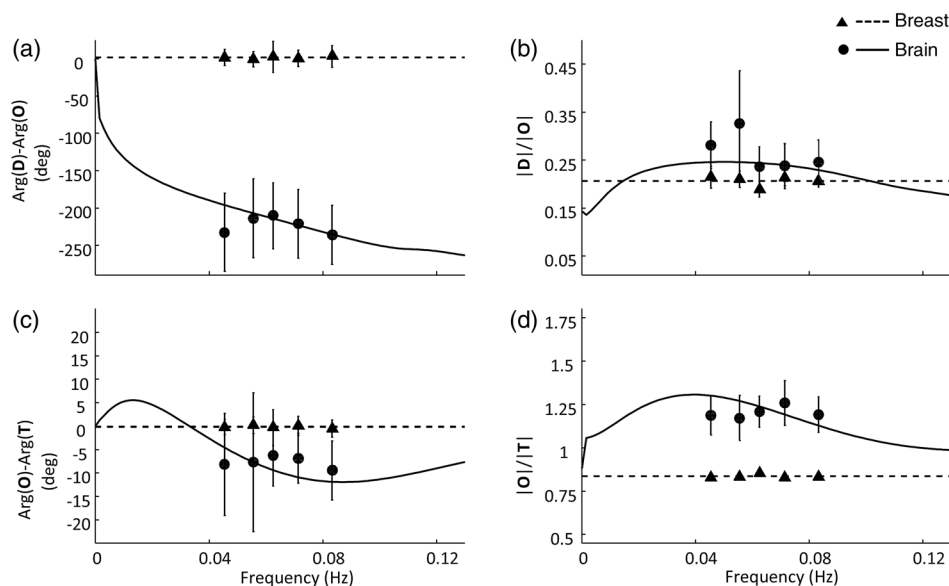


Fig. 3 Group-averaged CHS spectra measured on the brain (circles) and breast (triangles) of 11 human subjects at five frequencies of induced hemodynamic oscillations. The lines through the brain spectra (solid lines) are the best fits of the data with the hemodynamic model. The horizontal lines through the breast spectra (dashed lines) are at the average values over the five frequencies. (a) Phase difference $\text{Arg}(\mathbf{D}) - \text{Arg}(\mathbf{O})$; (b) amplitude ratio $|\mathbf{D}|/|\mathbf{O}|$; (c) phase difference $\text{Arg}(\mathbf{O}) - \text{Arg}(\mathbf{T})$; and (d) amplitude ratio $|\mathbf{O}|/|\mathbf{T}|$.

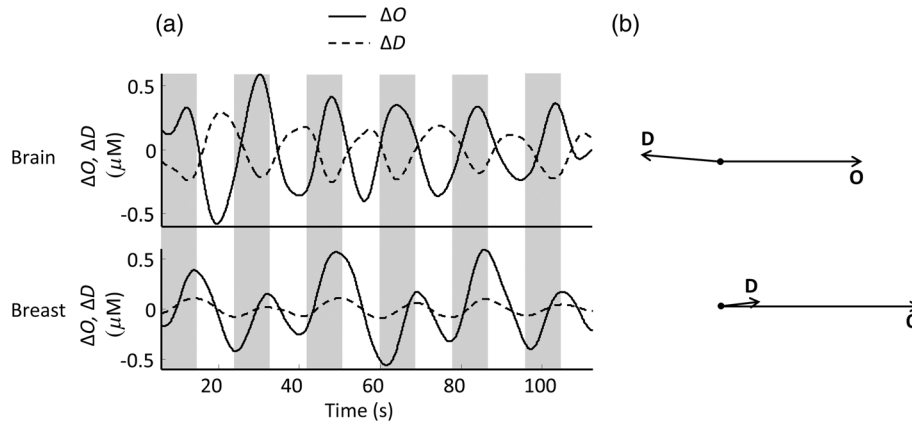


Fig. 4 (a) Time traces of changes in oxy- and deoxyhemoglobin concentrations (ΔO and ΔD , respectively) measured during the cyclic cuff occlusion protocol at 0.056 Hz for subject no. 1. The periods of time when the thigh cuffs were inflated are shaded. The top panel shows the out-of-phase behavior of O and D oscillations in the healthy brain. The bottom panel reports the breast data and shows the in-phase behavior of O and D oscillations in the healthy breast. (b) Phasor diagrams corresponding to the oscillations reported in (a). The phasor diagram in the top panel shows the out-of-phase O and D phasors in the healthy brain, whereas the one in the bottom panel shows the approximately in-phase O and D phasors in the healthy breast.

reproducibility of $t^{(c)}$ and $f_c^{(AR)}$ confirms the robustness of quantitative CHS measurements of cerebral blood flow (which is inversely related to $t^{(c)}$) and cerebral AR (whose effectiveness scales with $f_c^{(AR)}$).

The case of breast CHS spectra is qualitatively different. Because $\text{Arg}(\mathbf{O}) - \text{Arg}(\mathbf{T})$ and $\text{Arg}(\mathbf{D}) - \text{Arg}(\mathbf{O})$ are essentially zero, we can conclude that the blood volume oscillations are the dominant source of hemoglobin concentration oscillations. Therefore, oxy-, deoxy-, and total hemoglobin concentrations all oscillate in-phase. Under these conditions, $|\mathbf{O}|/|\mathbf{T}|$ specifies the average hemoglobin saturation of the volume-oscillating vascular compartments S_V , for which we found a value of $83\% \pm 1\%$ [see Fig. 3(d)]. We hypothesize that the highly compliant venous compartment provides the greatest contributions to these volume oscillations driven by blood pressure perturbations. This is similar to the case of spirometry, which was proposed to measure venous saturation from the blood volume oscillations associated with respiration (which also modulates ABP). In studies where spirometry was applied to skeletal muscles, the average venous saturation was found within the range 70% to 80%.^{17,21} In an NIRS study using venous occlusion to measure venous saturation in the human forearm, $S_V^{(v)}$ ranged from 50% to 80%.²² The value found by us for S_V in the breast is somewhat greater than the reported values of venous saturation in skeletal muscle. This result may be due to a different balance of blood flow and oxygen consumption in breast tissue compared with skeletal muscle or to greater contributions from the arterial compartment to S_V .

4 Discussion

The model described in Refs. 9 and 23 indicates that a pure blood flow oscillation induces a phase shift of π between D and O , whereas a pure blood volume oscillation induces synchronous oscillations of D and O . Equations 1 and 2, introduced in Sec. 2.2, are the analytical equations in the hemodynamic model that we used in order to solve for the six unknown parameters. By solving $\mathbf{D}(\omega)/\mathbf{O}(\omega)$ and $\mathbf{O}(\omega)/\mathbf{T}(\omega)$ instead of solving separately for the phasors $\mathbf{D}(\omega)$, $\mathbf{O}(\omega)$, and $\mathbf{T}(\omega)$, we can

cancel out unknown or frequency-dependent scaling factors for the amplitudes and phases of oscillations. However, to best explain the in-phase versus out-of-phase contributions from blood volume and blood flow oscillations, the equations for $\mathbf{D}(\omega)$ and $\mathbf{O}(\omega)$ are shown here as a sum of contributions from blood volume (subscript V), blood flow (subscript F), and oxygen consumption (subscript O)

$$\mathbf{O}(\omega) = \mathbf{O}_V(\omega) + \mathbf{O}_F(\omega) + \mathbf{O}_O(\omega) \quad (4)$$

$$\mathbf{D}(\omega) = \mathbf{D}_V(\omega) + \mathbf{D}_F(\omega) + \mathbf{D}_O(\omega) \quad (5)$$

Table 1 contains the terms and signs associated with each of the contributions.^{9,23} In the results reported here, we have assumed that there was no modulation of the cerebral metabolic rate (CMRO₂) or tissue oxygen consumption during the experiments. Table 1 (first and second rows) shows that an oscillation in any component (arterial, capillary, or venous) of the blood volume generates in-phase oscillations $\mathbf{O}_V(\omega)$ and $\mathbf{D}_V(\omega)$. Table 1 also shows that a given blood flow phasor $\mathbf{cbf}(\omega)$ (i.e., blood flow oscillations) generates phase-lagged oscillations $\mathbf{O}_F(\omega)$ [because of the negative phase of the complex factor in square brackets in the third row of Table 1 (for details, see Ref. 9)] and oscillations $\mathbf{D}_F(\omega)$ that are in opposition of phase with $\mathbf{O}_F(\omega)$ (because of the opposite sign of the terms in the third and fourth rows of Table 1). More precisely, even if blood volume and blood flow oscillations are in-phase, $\mathbf{O}_F(\omega)$ and $\mathbf{D}_F(\omega)$ are lagging behind $\mathbf{O}_V(\omega)$ and $\mathbf{D}_V(\omega)$. Note also that $\mathbf{O}_F(\omega)$ and $\mathbf{D}_F(\omega)$ are frequency-dependent, reflecting the nature of the low-pass filters associated with the capillary and venous compartments. A combination of both blood flow and blood volume oscillations induces frequency-dependent oscillations $\mathbf{O}(\omega)$ and $\mathbf{D}(\omega)$, which feature a relative phase that depends on the relative contributions of flow and volume oscillations, the blood transit time in the microvasculature, and the presence of any phenomena (such as AR mechanisms) that link flow and volume changes.

Figures 3(a) and 4 show that deoxy- and oxyhemoglobin oscillations are in-phase in the breast tissue and out-of-phase

Table 1 Contributions to $\mathbf{O}(\omega)$ and $\mathbf{D}(\omega)$ from oscillations in blood volume (subscript V) or blood flow (subscript F) at frequency ω . The oscillations in blood volume and blood flow are represented by the phasors $\mathbf{cbv}(\omega)$ and $\mathbf{cbf}(\omega)$, respectively. This table also shows the effect of oscillations in the metabolic rate of oxygen [phasor $\mathbf{cmro}_2(\omega)$] that are neglected in this work. ctHb is the concentration of hemoglobin in blood. Other symbols are defined in the text.

Term	Expression
$\mathbf{O}_V(\omega)$	$+ctHb[S^{(a)}CBV_0^{(a)}\mathbf{cbv}^{(a)}(\omega) + \langle S^{(c)} \rangle \mathcal{F}^{(c)}CBV_0^{(c)}\mathbf{cbv}^{(c)}(\omega) + S^{(v)}CBV_0^{(v)}\mathbf{cbv}^{(v)}(\omega)]$
$\mathbf{D}_V(\omega)$	$+ctHb[(1 - S^{(a)})CBV_0^{(a)}\mathbf{cbv}^{(a)}(\omega) + (1 - \langle S^{(c)} \rangle)\mathcal{F}^{(c)}CBV_0^{(c)}\mathbf{cbv}^{(c)}(\omega) + (1 - S^{(v)})CBV_0^{(v)}\mathbf{cbv}^{(v)}(\omega)]$
$\mathbf{O}_F(\omega)$	$+ctHb\left[\frac{\langle S^{(c)} \rangle}{S^{(v)}}((S^{(c)} - S^{(v)})\mathcal{F}^{(c)}CBV_0^{(c)}\mathcal{R}_{RC-LP}^{(c)}(\omega) + (S^{(a)} - S^{(v)})CBV_0^{(v)}\mathcal{R}_{G-LP}^{(v)}(\omega))\right][\mathbf{cbf}(\omega) - \mathbf{cmro}_2(\omega)]$
$\mathbf{D}_F(\omega)$	$-ctHb\left[\frac{\langle S^{(c)} \rangle}{S^{(v)}}((S^{(c)} - S^{(v)})\mathcal{F}^{(c)}CBV_0^{(c)}\mathcal{R}_{RC-LP}^{(c)}(\omega) + (S^{(a)} - S^{(v)})CBV_0^{(v)}\mathcal{R}_{G-LP}^{(v)}(\omega))\right][\mathbf{cbf}(\omega) - \mathbf{cmro}_2(\omega)]$

in the brain. This is an indication that the hemodynamics measured with NIRS are dominated by blood volume dynamics in healthy breast tissue, whereas they result from both blood volume and blood flow dynamics in brain tissue. We hypothesize that this contrasting behavior is due, at least in part, to a difference in the elastic properties of breast and brain tissues; in particular, the presence of the rigid skull limits the vascular expansion in brain tissue that, instead, is not constrained in breast tissue. Therefore, one may expect that the contributions of blood volume and blood flow to D and O are different in breast and brain tissues.

We observe that while the relative phase of D and O oscillations is related to the level of flow AR, one may not associate a lack of phase shift between D and O oscillations with a lack of AR. In fact, even in the absence of AR, when blood flow oscillations passively follow MAP oscillations so that the cerebral blood flow and MAP (and, to a first approximation, cerebral blood volume) are in-phase with each other, D and O oscillations are still, in general, out-of-phase with each other. This is because, as described in Sec. 1 and shown in Table 1, $\mathbf{O}_V(\omega)$ is in-phase with $\mathbf{cbv}(\omega)$, whereas $\mathbf{O}_F(\omega)$ lags behind $\mathbf{cbf}(\omega)$ as a result of the finite blood transit time in the microvasculature.

The phase relationship between D and O oscillations in breast tissue may be affected by the presence of breast cancer. Breast tumors have a larger elastic modulus than healthy breast tissue,²⁴ and they are also known to have an abnormal vasculature.²⁵ For both of these reasons, D and O oscillations in breast tumors may no longer be dominated by blood volume effects, as in healthy breast tissue, since the stiffer tissue and abnormal blood vessels may result in a less compliant tumor vasculature. Based on the model and results described here, D and O oscillations would become increasingly out-of-phase with each other as the contribution of blood volume oscillations decreases.

The in-phase oscillations of deoxy- and oxyhemoglobin in healthy breast tissue permitted us to compute the oxygen

saturation of hemoglobin in the volume-oscillating compartments, $S_V = |\mathbf{O}_V|/|\mathbf{T}|$, simply as the ratio $|\mathbf{O}|/|\mathbf{T}|$. To measure the saturation of the volume-oscillating compartments in the brain, one must take into account the blood flow contributions to the measured hemoglobin concentration. Kainerstorfer et al.²⁶ have described in detail how to account for contributions from blood flow in order to measure S_V in a general case where deoxy- and oxyhemoglobin oscillations are not in-phase with each other.

This work underlines the value of quantitative measurements of hemodynamic oscillations, be they induced by controlled perturbations in the ABP (as done here) or spontaneously occurring. However, in order to interpret such quantitative measurements of oscillatory hemodynamics, it is important to understand the dynamic relationship between the measured quantities (deoxy- and oxyhemoglobin concentrations in the case of NIRS) and the underlying physiological processes. In particular, this work highlights the qualitatively distinct behavior of different tissues (brain and breast) in response to the same systemic perturbation in ABP.

For noninvasive optical studies of the human brain, it is important to consider the fact that, in addition to brain tissue, extracerebral tissue (scalp, skull, and so on) also contributes to the measured optical signals. In relation to the study reported here, this means that extracerebral hemodynamics may act as a confounding factor for the cerebral hemodynamics that we intend to investigate and compare with breast tissue hemodynamics. However, while potentially confounding contributions from extracerebral hemodynamics may affect our measurements of the relative phase shift of O and D oscillations, they would not affect the main finding of this work that cerebral O and D oscillations are out-of-phase, whereas O and D oscillations in the healthy breast are in-phase. Nevertheless, in an effort to quantify the effect of extracerebral hemodynamics on our dynamic NIRS measurements, we are currently exploring the application of a two-layer diffusion model to discriminate superficial and deep-tissue hemodynamics.²⁷

5 Conclusion

This study has shown that blood-pressure-induced hemodynamic oscillations behave qualitatively differently in the healthy breast and in the healthy brain. Specifically, the different phase delays between D and O oscillations observed in the breast (~ 0 deg in the range 0.04 to 0.08 Hz) and the brain (~ -200 deg at 0.06 Hz) may be attributed to different relative contributions of blood flow and blood volume oscillations to the measured oxy- and deoxyhemoglobin concentrations. The situation may be different in pathologic conditions, which may affect the vascular compliance, the microvascular architecture, normal physiological mechanisms, and the elastic properties of tissue. In this case, a quantitative assessment of hemodynamic oscillations, possibly as a function of frequency as done in CHS, may offer diagnostically relevant information for pathologic conditions. The broad implications of this work are that CHS may be sensitive to perturbations to the integrity of the vasculature and hemodynamics in the brain (i.e., subarachnoid hemorrhage, traumatic brain injury, stroke, and so on) and in the breast (i.e., breast cancer). A thorough characterization of hemodynamic oscillations in tissue and their accurate interpretation can have a significant impact in the study of microvascular circulation and the assessment of its integrity.

Acknowledgments

We thank Anaïs Leproux, Michael Ghijsen, and Bruce Tromberg for useful discussions. This research was supported by the National Institutes of Health (Grant No. R01-CA154774).

References

1. M. Ferrari and V. Quaresima, "A brief review on the history of human functional near-infrared spectroscopy (fNIRS) development and fields of application," *Neuroimage* **63**(2), 921–935 (2012).
2. B. J. Tromberg et al., "Assessing the future of diffuse optical imaging technologies for breast cancer management," *Med. Phys.* **35**(6), 2443–2451 (2008).
3. S. Fantini and A. Sassaroli, "Near-infrared optical mammography for breast cancer detection with intrinsic contrast," *Ann. Biomed. Eng.* **40**(2), 398–407 (2012).
4. M. Reinhard et al., "Spatial mapping of dynamic cerebral autoregulation by multichannel near-infrared spectroscopy in high-grade carotid artery disease," *J. Biomed. Opt.* **19**(9), 097005 (2014).
5. R. Aaslid et al., "Asymmetric dynamic cerebral autoregulatory response to cyclic stimuli," *Stroke* **38**(5), 1465–1469 (2007).
6. J. A. H. R. Claassen, B. D. Levine, and R. Zhang, "Dynamic cerebral autoregulation during repeated squat-stand maneuvers," *J. Appl. Physiol.* **106**, 153–160 (2009).
7. M. Reinhard et al., "Oscillatory cerebral hemodynamics—the macro- vs. microvascular level," *J. Neurol. Sci.* **250**, 103–109 (2006).
8. M. L. Piero et al., "Phase-amplitude investigation of spontaneous low-frequency oscillations of cerebral hemodynamics with near-infrared spectroscopy: a sleep study in human subjects," *Neuroimage* **63**(3), 1571–1584 (2012).
9. S. Fantini, "Dynamic model for the tissue concentration and oxygen saturation of hemoglobin in relation to blood volume, flow velocity, and oxygen consumption: implications for functional neuroimaging and coherent hemodynamics spectroscopy (CHS)," *Neuroimage* **85**, 202–221 (2014).
10. C. H. Schmitz et al., "Design and implementation of dynamic near-infrared optical tomographic imaging instrumentation for simultaneous dual-breast measurements," *Appl. Opt.* **44**(11), 2140–2153 (2005).
11. S. A. Carp et al., "Dynamic functional and mechanical response of breast tissue to compression," *Opt. Express* **16**(20), 16064–16078 (2008).
12. C. M. Carpenter et al., "Inspired gas-induced vascular change in tumors with magnetic-resonance-guided near-infrared imaging: human breast pilot study," *J. Biomed. Opt.* **15**(3), 036026 (2010).
13. M. L. Flexman et al., "Optical biomarkers for breast cancer derived from dynamic diffuse optical tomography," *J. Biomed. Opt.* **18**(9), 096012 (2013).
14. T. Parks and J. McClellan, "Chebyshev approximation for nonrecursive digital filters with linear phase," *IEEE Trans. Circuit Theory* **19**(2), 189–194 (1972).
15. B. Boashash, "Estimating and interpreting the instantaneous frequency of a signal—part 1: fundamentals," *Proc. IEEE* **80**(4), 520–538 (1992).
16. M. L. Piero et al., "Reduced speed of microvascular blood flow in hemodialysis patients versus healthy controls: a coherent hemodynamics spectroscopy study," *J. Biomed. Opt.* **19**(2), 026005 (2014).
17. M. L. Piero et al., "Validation of a novel hemodynamic model for coherent hemodynamics spectroscopy (CHS) and functional brain studies with fNIRS and fMRI," *Neuroimage* **85**, 222–233 (2014).
18. J. M. Kainerstorfer, A. Sassaroli, and S. Fantini, "Coherent hemodynamics spectroscopy in a single step," *Biomed. Opt. Express* **5**(10), 3403–3616 (2014).
19. J. M. Kainerstorfer et al., "Practical steps for applying a new dynamic model to near-infrared spectroscopy measurements of hemodynamic oscillations and transient changes: implications for cerebrovascular and functional brain studies," *Acad. Radiol.* **21**(2), 185–196 (2014).
20. J. H. Zar, "Circular distributions," in *Biostatistical Analysis*, 5th ed., pp. 612–623, Pearson Prentice Hall, Upper Saddle River, New Jersey (2010).
21. M. A. Franceschini et al., "Near-infrared spirometry: noninvasive measurements of venous saturation in piglets and human subjects," *J. Appl. Physiol.* **92**, 372–384 (2002).
22. C. W. Yoxall and A. M. Weindling, "Measurement of venous oxyhaemoglobin saturation in the adult human forearm by near infrared spectroscopy with venous occlusion," *Med. Biol. Eng. Comput.* **35**, 331–336 (1997).
23. S. Fantini, "A new hemodynamic model shows that temporal perturbations of cerebral blood flow and metabolic rate of oxygen cannot be measured individually using functional near-infrared spectroscopy," *Physiol. Meas.* **35**(1), N1–N9 (2014).
24. A. Samani, J. Zubovits, and D. Plewes, "Elastic moduli of normal and pathological human breast tissues: an inversion-technique-based investigation of 169 samples," *Phys. Med. Biol.* **52**(6), 1565–1576 (2007).
25. P. Vaupel, F. Kallinowski, and P. Okunieff, "Blood flow, oxygen and nutrient supply, and metabolic microenvironment of human tumors: a review," *Cancer Res.* **49**(23), 6449–6465 (1989).
26. J. M. Kainerstorfer, A. Sassaroli, and S. Fantini, "Optical oximetry of volume-oscillating vascular compartments: contributions from oscillatory blood flow," *J. Biomed. Opt.* **21**(10), 101408 (2016).
27. S. Fantini et al., "Non-invasive assessment of cerebral microcirculation with diffuse optics and coherent hemodynamics spectroscopy," *Proc. SPIE* **9690**, 96900S (2016).

Biographies for the authors are not available.